Capturing Different Intermediate Phases during Zeolite Synthesis

Jinjin Zeng,† German Sastre,‡ and Suk Bong Hong†,*

† Center for Ordered Nanoporous Materials Synthesis, Division of Environmental Science and Engineering, POSTECH, Pohang 37673, Korea.

‡ Instituto de Tecnologia Quimica (UPV-CSIC), Universidad Politécnica de Valencia, Av. Naranjos s/n, Valencia 46022, Spain.

ABSTRACT: Despite extensive efforts over the past several decades, the current mechanistic understanding of zeolite crystallization is still far from satisfactory, thus precluding the synthesis of designer zeolites. Here we show that the nucleation and in situ transformation pathways during the synthesis of the medium-pore zeolite TNU-9 can be altered by controlling the extent of cooperative structure direction between Na^+ and Cs^+ ions in the presence of 1,4-bis(*N*-methylpyrrolidinium)butane cations as an organic structure-directing agent. The intermediate phase selectivity was found to change from bikitaite to analcime to layered MCM-22 precursor when the gel Na/Cs ratio was adjusted to 7, 15, and 20, respectively. We also show that the transformation of bikitaite into TNU-9 begins at the surface of intermediate crystals, unlike that of analcime and MCM-22 precursor by a dissolution-recrystallization process. The force field simulation results suggest that the nucleation of different intermediate phases is not thermodynamically but kinetically controlled. This study provides a new basis for advancing the fundamental understanding of zeolite crystallization pathways.

■ INTRODUCTION

Zeolites are crystalline microporous aluminosilicates with commercial uses in catalysis, ion exchange, adsorption, and separation.[1,2] Nevertheless, the rational design and synthesis of zeolites with finely tuned physicochemical properties for particular applications are still far from reality, primarily due to the lack of a solid understanding of the mechanisms involved in their crystallization.[3-9]

Although many hypotheses have been proposed to explain zeolite crystallization so far, there is a general consensus that this complex self-assembly process is triggered by a nucleation of discrete embryo-like structures with the identity of the crystallizing phase.[3-9] On the other hand, zeolites are metastable in nature. Thus, the in situ transformation of one phase into another has often been observed, at the expense of the former during hydrothermal zeolite synthesis. The classic example is the formation of zeolite Y (framework type FAU) during the synthesis of another large-pore zeolite ZSM-4 (MAZ) using Na^+ and tetramethylammonium ions as inorganic and organic structure-directing agents (SDAs), respectively.[10] The considerations made so far suggest that the free energy or structure of zeolite precursors in the amorphous synthesis mixture might be similar to that of the phase crystallized earliest.[11-13] However, little or no attention has been paid to whether and how the nucleation and/or transformation pathways in the crystallization process of zeolites with a particular framework topology can be controlled.

The present study addresses these issues from both thermodynamic and kinetic points of view, with the aim of elucidating the exact roles of synthesis components, especially inorganic and organic SDAs, in the formation of intermediate and final zeolite phases. We revisit the synthesis of the high-silica medium-pore zeolite TNU-9 (TUN),[14-16] because a disordered MCM-22 (MWW) precursor (MCM-22(P)) is first formed over narrow ranges of gel Si/Al and Na/Al ratios in the presence of diquaternary 1,4-bis(*N*-methylpyrrolidinium)butane (1,4-MPB^{2+}) ions.[16-18] To intentionally induce the formation of intermediate phases other than MCM-22(P) before TNU-9 crystallization, we apply the multiple inorganic cation approach that has been shown to be effective in promoting a synergy between different types of inorganic SDAs in the search for novel zeolite structures.[19-25] Here the Cs^+ ion was selected as the second inorganic SDA, because the structure-directing properties of this alkali cation with a weak salting-out power are significantly different from those of Na^+. It has long been recognized that the Na^+ ion has the ability to order water molecules, thus the structure-forming role, whereas the Cs^+ ion interacts less with water molecules, resulting in breaking of the structure.[3,26,27] Our findings reveal the existence of bikitaite (BIK) and analcime (ANA) as another two intermediates of TNU-9.

■ RESULTS AND DISCUSSION

Synthesis. We have found more than eight new ordered or disordered zeolites via a multiple inorganic approach over the last decade.[19-25] This synthesis approach generally includes the use of a rather small amount (less than half) of organic SDAs at relatively lower gel Si/Al ratios (≤ 10) compared to the original gel composition (Si/Al = 20-30) for TNU-9[15,16] to enhance the cooperative structure-directing effects of inorganic SDAs. For example, we synthesized PST-32, a thermally stable version of the large-pore phosphate-based molecular sieve UCSB-10 (SBT), using an aluminosilicate (Si/Al = 5.0) gel containing 1,4-dimethyl-1,4-diazonia-bicyclo[2,2,2]octane (Me_2-DABCO) dihydroxide as an organic SDA and both Na^+ and Cs^+ ions (Na/Cs = 7) as inorganic SDAs.[23,24] Therefore, we started our TNU-9 synthesis at 150 ℃ after replacing Me_2-DABCO$(OH)_2$ with an equimolar amount of

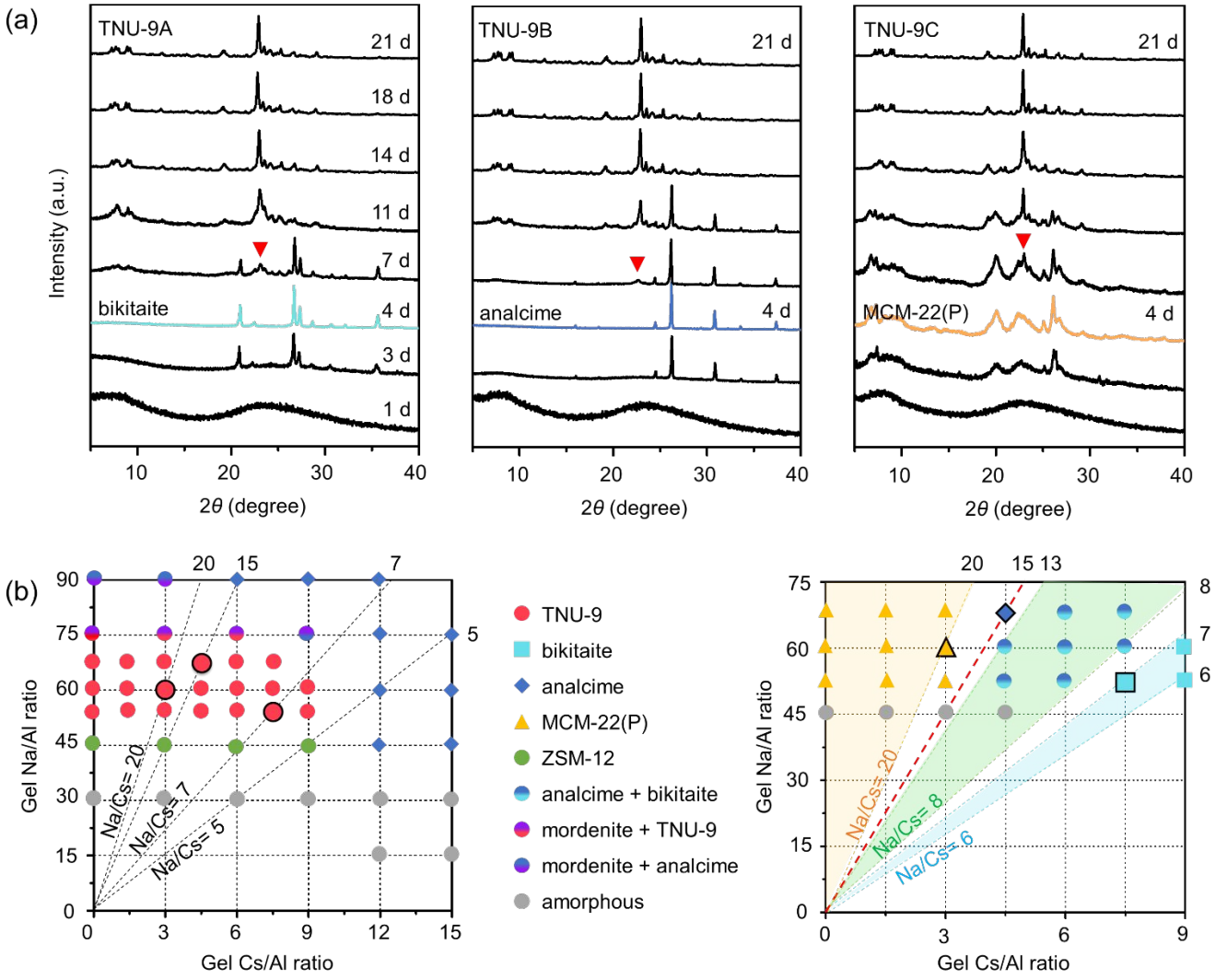

Figure 1. (a) PXRD patterns of a series of solid products isolated as a function of time during TNU-9 synthesis under static conditions at 150 °C, using aluminosilicate gels with the same Si/Al ratio (50) but different Na/Al and Cs/Al ratios: 0.75(1,4-MPB)O·5.25Na_2O·0.75Cs_2O·0.3Al_2O_3·30SiO_2·300H_2O (left), 0.75(1,4-MPB)O·6.75Na_2O·0.45Cs_2O·0.3Al_2O_3·30SiO_2·300H_2O (middle), and 0.75(1,4-MPB)O·6.00Na_2O·0.30Cs_2O· 0.3Al_2O_3·30SiO_2·300H_2O (right). The X-ray peak around $2\theta = 22.9°$ due to the TUN 151 reflection is marked by an inverted triangle. (b) Solid products isolated after heating 1,4-MPB^{2+}-containing gels with the same Si/Al ratio (50) but different Na/Al and Cs/Al ratios at 150 °C for 21 (left) and 4 (right) days, respectively. The points corresponding to the three pairs of fully characterized (Table 1) intermediate (right) and final (left) products are highlighted with black borders. The mixture products are denoted as split symbols, and all amorphous phases remained unchanged up to 21 days.

1,4-$MPB(OH)_2$. No TNU-9 was detected when the synthesis was carried out using gels with Si/Al ratios < 25 under static conditions for 21 days. However, we were able to obtain pure TNU-9 at a gel Si/Al ratio of 50 (Table S1). A further increase in Si/Al ratio to 100 gave MCM-47, a layered material consisting of ferrierite (FER) sheets,[27] as a major phase.

We next examined the crystallization kinetics of TNU-9 at the above gel composition (Si/Al = 50, Na/Al = 53, and Na/Cs = 7). Interestingly, the one-dimensional (1D) small-pore zeolite bikitaite[29] appeared as a new intermediate phase that fully crystallized after 4 days of heating at 150 ℃ (Figure 1a). This led us to investigate the effects of gel Na/Al and Cs/Al ratios on the synthesis of TNU-9 in the presence of 1,4-MPB^{2+}. When the Na/Cs ratio was fixed to 7, the Na/Al and Cs/Al ratio ranges leading to pure TNU-9 were found to be narrow (53 – 60 and 7.5 – 9.0, respectively). However, while a decrease in Na/Cs ratio to 5.0 yielded only the 1D large-pore zeolite ZSM-12 (MTW), an increase in Na/Cs ratio from 7 to infinity led to pure TNU-9 in the wider Na/Al and Na/Cs ratios ranges of 53 – 68 and 0 – 7.5 (left diagram in Figure 1b). This indicates that the Cs^+ concentration in the gel should be kept below a certain level to crystallize TNU-9.

To identify whether all TNU-9 samples purely synthesized here have intermediate phases other than bikitaite, we characterized the solid products isolated after heating their synthesis gels at 150 °C for 4 days by powder X-ray diffraction PXRD) and found that the small-pore zeolite analcime (ANA) was another new intermediate (Figure 1a), although it was obtained purely at a specific gel composition (Na/Al = 68, Cs/Al = 4.5, and Na/Cs = 15). We also observed MCM-22(P) at wider Na/Cs ratios of 20-∞ (right diagram in Figure 1b).

Table 1. Chemical Composition Data of Intermediate and TNU-9 Zeolites Synthesized in This Study[a]

sample ID	IZA code	phase	unit cell composition	Si/Al ratio[b]	(Na+Cs)/Al ratio[b]	Na/Cs ratio[b]
PST-36	BIK	intermediate	$\|Na_{0.1}Cs_{0.9}(H_2O)_{2.8}\|_{1/2}[Al_{1.0}Si_{11.0}O_{24}]_{1/2}$	11.0 (50)	1.0 (20)	0.1 (7)
TNU-9A	TUN	final product	$\|Na_{1.3}Cs_{0.2}(1,4\text{-MPB})_{7.8}(OH)_{5.4}(H_2O)_{11.2}\|[Al_{11.7}Si_{180.3}O_{384}]$	15.4	0.13	6.5
PST-37	ANA	intermediate	$\|Na_{3.6}Cs_{2.8}(H_2O)_{23.5}\|[Al_{6.4}Si_{41.6}O_{96}]$	6.5 (50)	1.0 (24)	1.3 (15)
TNU-9B	TUN	final product	$\|Na_{1.8}Cs_{0.2}(1,4\text{-MPB})_{8.1}(OH)_{6.5}(H_2O)_{11.5}\|[Al_{11.7}Si_{180.3}O_{384}]$	15.4	0.17	9.0
MCM-22(P)[c]	-	intermediate	$\|Na_{0.2}Cs_{0.1}(1,4\text{-MPB})_{4.0}(OH)_{3.0}(H_2O)_{22.0}\|[Al_{5.3}Si_{66.7}O_{144}]$	12.6 (50)	0.06 (21)	2.0 (20)
TNU-9C	TUN	final product	$\|Na_{2.8}Cs_{0.2}(1,4\text{-MPB})_{8.0}(OH)_{9.5}(H_2O)_{8.9}\|[Al_{9.5}Si_{182.5}O_{384}]$	19.2	0.32	14

[a]Determined by elemental and thermal analyses. [b]The values in parentheses are the ratios of each synthesis gel. [c]The unit cell was assumed to be the same as that of the MWW structure with 72 T-atoms.

Therefore, it is clear that the structure type of intermediates formed during TNU-9 synthesis in the presence of 1,4-MPB^{2+} is strongly dependent on the gel Na/Cs ratio. This demonstrates that the nucleation and transformation pathways of TNU-9 can be altered when the extent of cooperation between the structure-forming Na^+ and structure-breaking Cs^+ ions is carefully controlled.

The framework density (FD), defined by the number of T-atoms per 1000 Å^3, of the fully connected three-dimensional (3D) MCM-22 structure is 15.9.[29] Thus, the layered precursor MCM-22(P) should have an FD value below this. Given that the FD value of TNU-9 is 17.6, its crystallization at the expense of MCM-22(P) can be explained by Ostwald ripening.[30] On the other hand, our theoretical calculation results show that bikitaite and analcime with FD values of 18.7 and 19.2, respectively, are thermodynamically unstable compared to the lower-density zeolite TNU-9 (Table 2). This implies that their transformation into TNU-9 also occurs by an Ostwald ripening process. It is interesting to note that bikitaite and MCM-22(P) synthesized here have similar Si/Al ratios but substantially different extra-framework compositions (Table 1), suggesting the profound effect of extra-framework species in an intermediate zeolite phase on the transformation into the more stable zeolite product.[31]

Gel alkalinity is another crucial factor influencing zeolite nucleation and growth kinetics.[6] Therefore, we replaced the hydroxide form of 1,4-MPB^{2+} with its bromide one and performed zeolite syntheses under the three conditions, in which pure bikitaite, analcime, and MCM-22(P) appeared prior to TNU-9 formation (Figure 1a). Despite the small decrease ($\leq$ 0.2) in initial gel pH, bikitaite always emerged as an intermediate phase at Na/Cs = 7-20. Furthermore, ZSM-12, but not TNU-9, was the final product obtained after 21 days at 150 °C (Table S1 and Figure S1). It should be noted that none of the four ZSM-12 zeolites from gels with Na/Al = 45 and Cs/Al = 0-9 (left diagram in Figure 1b) had intermediate phases before their crystallization.

IM-5 (IMF) and NU-88 are high-silica medium-pore and large-pore zeolites that can be synthesized using 1,5-bis(*N*-methylpyrrolidinium)pentane (1,5-MPP) and 1,6-bis(*N*-methylpyrrolidinium)hexane (1,6-MPH) ions as an organic SDA in the presence of Na^+ ions, respectively.[32-34] Thus, they constitute a synthesis series with TNU-9 because the organic SDA differs only in the length of the methylene bridging unit. This led us to replace 1,4-MPB^{2+} with the equivalent amount of 1,5-MPP^{2+} and 1,6-MPH^{2+} to examine whether any intermediate exists before the formation of IM-5 and NU-88 under the above three conditions. Both organic SDAs led to the emergence of bikitaite at Na/Cs = 7, respectively (Table S1 and Figure S2), like 1,4-MPB^{2+}. However, when the gel Na/Cs ratio increased to 20, neither produced crystalline intermediates. Therefore, since 1,4-MPB^{2+} directed the synthesis of MCM-22(P) at the same gel Na/Cs ratio (Figure 1a), it is clear that not only the final phase selectivity but also the nucleation pathway in zeolite synthesis can be altered by the type of organic SDAs employed.

Characterization. Table 1 lists the unit cell compositions of three pairs of intermediate and TNU-9 zeolites synthesized here (Figure 1a). Here we assumed that MCM-22(P) has the same unit cell composition as that of as-synthesized 3D MWW, because its crystallographic structure remains unknown. The composition data in Table 1 reveal that the Si/Al ratios (11.0 and 6.5, respectively) of our bikitaite and analcime, as well as their synthesis gel compositions, are significantly different from those reported so far for both materials.[29,35,36] This is particularly true for the latter zeolite whose Si/Al ratio is the highest among the reported ANA-type zeolites. Therefore, we refer to bikitaite and analcime obtained in this study using our laboratory codes PST-36 and PST-37. The higher Si/Al ratio of PST-36 compared to PST-37 can be rationalized by considering its significantly higher proportion (90 vs 44%) of extra-framework Cs^+ ions with a weak salting-out power[27] (Table 1).

^{27}Al MAS NMR shows only one line around 58 ppm (Figure 2a), typical of tetrahedral Al in the zeolite framework. Attempts to deconvolute their ^{29}Si MAS NMR spectra by assigning each of the four Si(*n*Al) lines with n = 3, 2, 1, and 0 as a single Si environment gave $(Si/Al)_{NMR}$ ratios of 11.0 and 6.2 for PST-36 and PST-37 with two and one crystallographically T-sites, respectively[29] (Figure 2b), in excellent agreement with those obtained from elemental analysis. ^{29}Si MAS NMR also shows that the bikitaite appearing as an intermediate during the crystallization of ZSM-12 has a $(Si/Al)_{NMR}$ ratio of 12.5, which is slightly higher than that (11.0) of PST-36 (Figure S3). Elemental analysis indicates that the two TNU-9 zeolites, which have PST-36 and PST-37 as an intermediate (labelled as TNU-9A and TNU-9B, respectively), are characterized by the same Si/Al ratio (15). However, the zeolite obtained through the MCM-22(P) route (TNU-9C) has a higher Si/Al ratio of 19 (Table 1), which can be further supported by the slightly weaker relative intensity of its ^{29}Si line around −103 ppm assignable to Si(1Al) species (Figure S4).

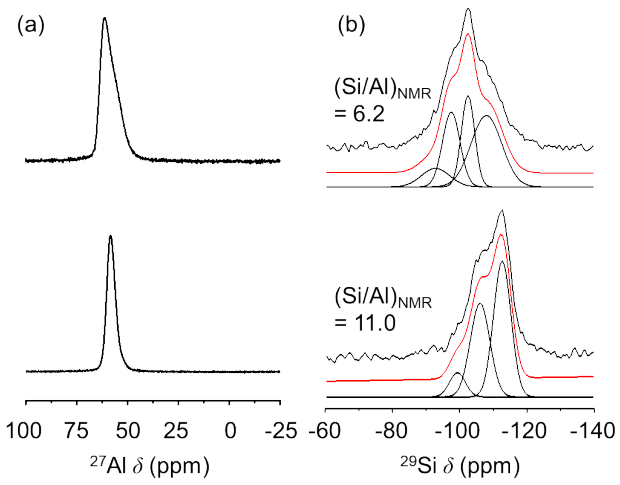

Figure 2. (a) and (b) ^{27}Al (left) and ^{29}Si (right; experimental (top), simulated (middle), and deconvoluted components (bottom)) MAS NMR spectra of as-synthesized PST-36 (bottom) and PST-37 (top).

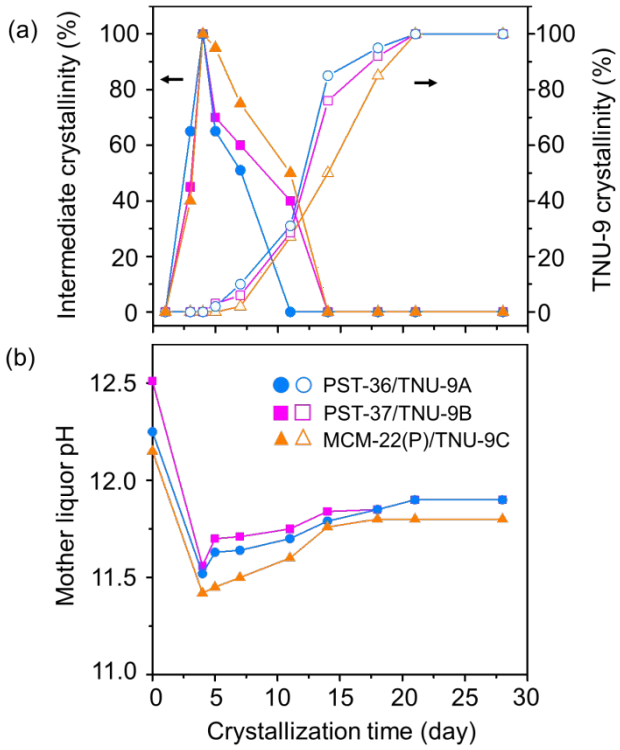

Figure 3. (a) Crystallinities of intermediates and final product TNU-9 and (b) pH values of their mother liquors as a function of crystallization time from three different gel compositions (see Figure 1a) under static conditions at 150 °C.

The replacement of 1,4-MPB(OH)$_2$ with a combination of NaOH and CsOH while keeping the gel Na/Cs ratios at 7 and 15, respectively, under the optimized conditions for the synthesis of PST-36 and PST-37, always led to a mixture of layered kenyaite and magadiite materials (Table S1). This implies that 1,4-MPB^{2+} is required for crystallizing these two small-pore zeolites, but not present within their pores (Table 1). Therefore, considering the absence of host-guest interactions, we define the role of 1,4-MPB^{2+} in the crystallization of PST-36 and PST-37 as a spectator or structure-spectating agent rather than as an SDA. In addition, although there is a significant enrichment of Cs^+ in both zeolites with respect to their gels, the extent of enrichment was found to be about six times higher for PST-36 than for PST-37. This suggests the higher preference of Cs^+ for the formation of a BIK structure. However, the role of 1,4-MPB^{2+} as an SDA in the crystallization of MCM-22(P), as well as TNU-9, is quite clear (Table 1 and Figure S5).

When comparing the crystallization kinetics of PST-36, PST-37, and MCM-22(P) at 150 °C, on the other hand, there are no notable differences in the time needed to achieve full crystallization. However, the intermediate transformation rate was faster in the order MCM-22(P) < PST-37 < PST-36 (Figure 3a). This is expected because a more siliceous phase is more stable in the crystallization medium. We also noticed a sharp pH rise after 4 days during the transformation of PST-36 and PST-37 into TNU-9 with exceedingly high contents of inorganic SDAs compared to the MCM-22(P), which is in line with their faster dissolution rate at 4-5 days (Figure 3b).

The field-emission scanning electron microscopy (FE-SEM) image of PST-37 crystals, obtained after heating a gel with Na/Al = 68, Cs/Al = 4.5, and Na/Cs = 15 at 150 °C for 4 days, appeared as agglomerated spheres with a diameter of ca. 8 μm (Figure 4a). However, when the crystallization time increased to 11 days, two different crystal morphologies were observed. A further increase to 21 days led to only rod-like crystals that are ca. 1.0 μm in length and 0.3 μm in diameter, typical of TNU-9 morphology. The same trend was observed during the transformation of MCM-22(P) into TNU-9 (Figure 4b). Therefore, the transformation of PST-37 with ANA topology, as well as MCM-22(P), into TNU-9 is solution-mediated, as previously reported.[16]

However, the transformation of PST-36 with BIK topology is substantially different from such a dissolution-recrystallization, because its morphology, i.e., star-shaped particulates of 10-15 μm, which in turn consist of densely packed plates of < 0.1 μm in thickness, generally remained until TNU-9 fully crystallized (Figure 4c). A closer look at the surface of the particulates isolated after 7 days revealed the appearance of tiny crystals attached to the surface of the thin plates, unlike the smooth-surfaced PST-36 crystals. In particular, the serendipitously imaged cross section of a particulate isolated after 11 days showed that while the interior of this particulate was densely packed with rectangular parallelepipeds, its external surface was covered by isomorphic but considerably bigger crystals. These results indicate that the nucleation pathway begins by a surface dissolution of the PST-36 crystals to serve as Si and Al sources for TNU-9 crystallization, where the organic SDA (1,4-MPB^{2+}) should be supplied from the mother liquor. A similar conclusion can also be drawn from the transformation of bikitaite into ZSM-12 (Figures S1 and S3). Therefore, the transformation mechanism of intermediates into the final zeolite product can differ according to their structure type.

To gain thermodynamic insights into the transformation of PST-36, PST-37, and MCM-22(P) during TNU-9 synthesis, we calculated the synthesis energies of these three intermediate phases, as well as of TNU-9A (or TNU-9B) and TNU-9C zeolites with different Si/Al ratios (15 and 19, respectively),

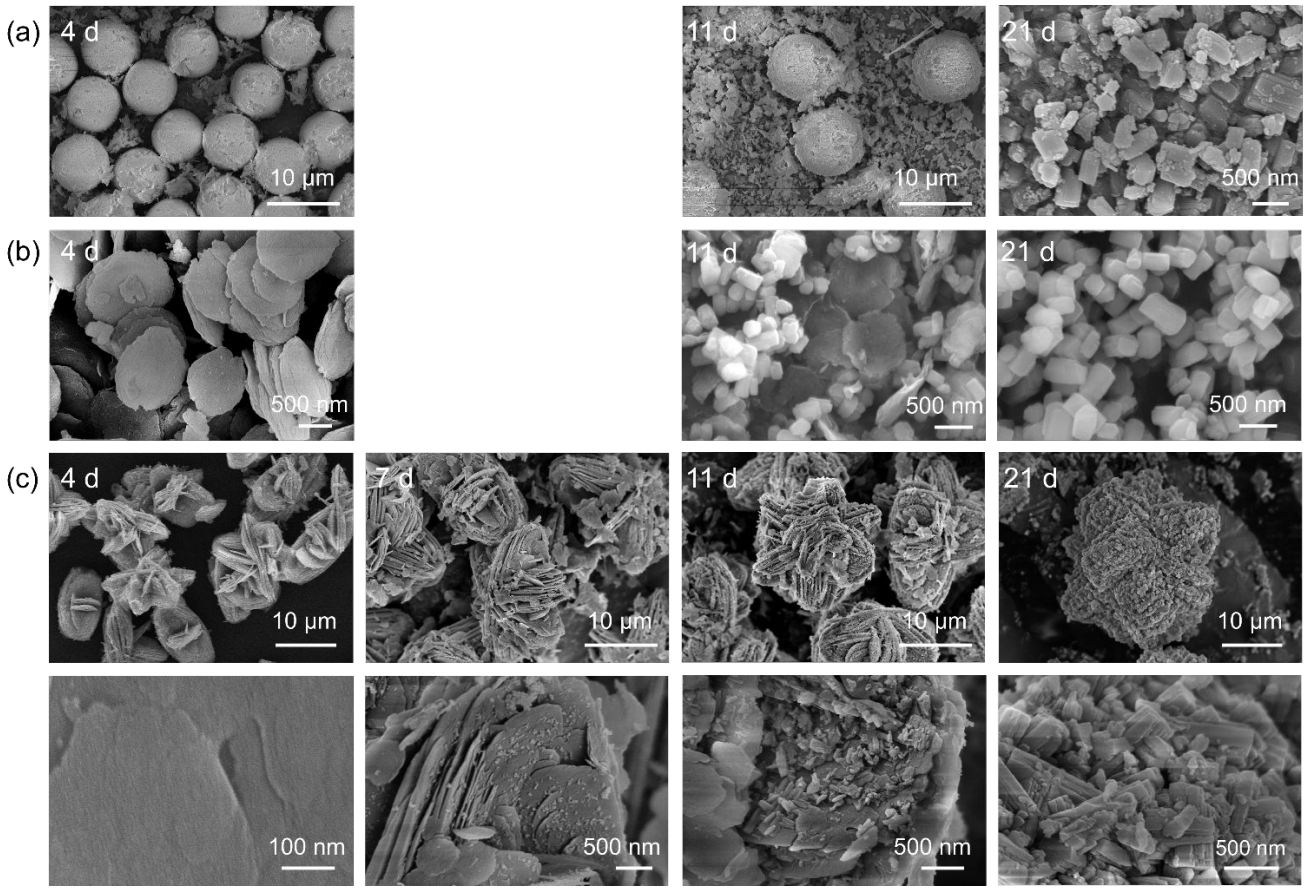

Figure 4. FE-SEM images of solid products isolated at different crystallization times during TNU-9 synthesis at 150 °C, where the intermediate phase is (a) PST-37, (b) MCM-22(P), and (c) PST-36, respectively (see Figure 1a for gel compositions)

Table 2. Calculated Synthesis Energies per 192 T-atom unit cell of Three Pairs of Intermediate and TNU-9 Zeolites[a]

pair	$E_{syn,Inter}$[b] (eV)	$E_{syn,TNU-9}$[b] (eV)	ΔE_{syn}[b] (eV)
PST-36/TNU-9A	-39376.5 (-68.362)	-40581.8 (-70.455)	-1205.3 (-2.093)
PST-37/TNU-9B	-37537.5 (-65.169)	-40581.8 (-70.455)	-3044.3 (-5.286)
MCM-22(P)/TNU-9C	-38774.3 (-67.316)	-40652.9 (-70.578)	-1878.6 (-3.262)

[a]$E_{syn,Inter}$, synthesis energy of each intermediate; $E_{syn,TNU-9}$, synthesis energy of TNU-9; $\Delta E_{syn} = E_{syn,TNU-9} - E_{syn,Inter}$. [b]The values in parentheses are the synthesis energies per T-atom.

according to the procedure employed in recent work.[37,38] To do so, we developed five equations (Supporting Information Text, Tables S2 and S3, and Figure S6) for the formation of the experimentally characterized intermediate and final products in Table 1. Since the synthesis energy gives an estimation of how the internal energy of the system evolves from synthesis gels to zeolite products, it is convenient to adjust the equations to a common gel composition so that a comparison of the energies of the crystallized products shows their relative stability.

Table 2 compares the calculated synthesis energies of three intermediate/TNU-9 pairs described above. Because of their energetic contribution to the oligomerization and ring closure reactions during zeolite synthesis, we included the energies of $Si(OH)_4$, $Al(OH)_3$, and H_2O (-61.4015, -40.2611, and -12.8344 eV, respectively) in the calculations.[37] The results show that the synthesis energy of TNU-9 is considerably lower than that of each intermediate, rationalizing the structure-directing role of 1,4-MPB^{2+} ions. Our recent synthesis energy calculations of more than 20 zeolites with different framework structures and/or Al contents directly synthesized from amorphous gels containing various organic SDAs have revealed that the synthesis energy per T-atom is always lower than ca. -1.4 eV.[37,38] We note here that the difference in the synthesis energy per T-atom of each intermediate and TNU-9 pair is higher than -2.0 eV (Table 2). In particular, significant differences (ca. 3.2 eV) in the synthesis energies per T-atom of three different intermediates suggest that the intermediate nucleation may be kinetic in nature, rather than thermodynamic.

■ CONCLUSION

In summary, we found two new intermediate phases (high-silica BIK- and ANA-type zeolites), as well as the already known MCM-22(P) phase, during the synthesis of medium-pore TNU-9 zeolite by controlling the extent of cooperation between the structure-forming Na^+ and structure-breaking Cs^+ ions, i.e., the

Na/Cs ratio of synthesis gels, in the presence of 1,4-MPB^{2+} ions as an unselective SDA. We also identified 1,4-MPB^{2+} as a structure-spectating agent rather than as an SDA in the nucleation and growth of the former two intermediates. More interestingly, the transformation pathway of intermediates during TNU-9 synthesis was found to be dependent on their structure type. This study provides valuable insights into how the nucleation and growth pathways in zeolite crystallization can be controlled and will inspire future efforts aimed at the rational synthesis of novel zeolite structures and/or compositions.

■ EXPERIMENTAL SECTION

Zeolite Synthesis and Characterization. The hydroxide and bromide forms of 1,4-MPB^{2+}, 1,5-MPP^{2+}, and 1,6-MPH^{2+} ions were prepared according to the procedures described elsewhere.[16,34] The other reagents included NaOH (50%, Aldrich), NaBr (99.8%, Aldrich), CsOH (50%, Aldrich), sodium aluminate ($1.0Na_2O{\cdot}1.0Al_2O_3$, 99%, Strem), and colloidal silica (Ludox HS-40, 40%, Aldrich). The final composition of the synthesis mixture was $0.75RO{\cdot}xNa_2O{\cdot}yCs_2O{\cdot}zAl_2O_3{\cdot}\ 30SiO_2{\cdot}300H_2O$, where R is 1,4-$MPB^{2+}$, 1,5-$MPP^{2+}$, or 1,6-$MPH^{2+}$, and x, y and z are between $4.5 \le x \le 9.0$, $0 \le y \le 1.5$, and $0 \le z \le 3.0$, respectively. After being stirred at room temperature for 1 day, the final gel was heated under static conditions at 150 °C (if required, at 175 °C) for 1-28 days.

As-synthesized zeolites were characterized by PXRD, elemental and thermal analyses, FE-SEM, and ^{27}Al and ^{29}Si MAS NMR spectroscopy, as described in our previous study.[16] The crystallinity of a series of the products isolated as a function of crystallization time from different gel compositions was determined by comparing the area of an intense X-ray peak around 2θ = 26.7, 26.2, 26.1, and 22.9°, corresponding to the BIK (002), ANA (400), MWW (310), and TUN (151) reflections, respectively, with that of each of the fully crystallized sample. No special care was taken to eliminate preferred orientation effects on the PXRD pattern of the respective product crystals, whereas the same amount of sample was loaded in the sample holder for all measurements. The yield of each solid product was calculated by dividing the weight of solid obtained at different crystallization times by the total weight of the anhydrous oxide form of the synthesis gel.

Computational Methods. The crystallographic data of the ANA, BIK, TUN and MWW unit cells were extracted from the Database of Zeolite Structures created by the Structure Commission of the International Zeolite Association.[29] The location and number of ions (1,4-MPB^{2+}, Na^+, Cs^+, or OH^-) and H_2O molecules inside the zeolite pores were optimized using the zeoTsda software and the latest version of our developed force field for synthesis of aluminosilicate zeolites, including $Si(OH)_4$ and $Al(OH)_3$.[39,40] 20 random Al distributions were generated for each zeolite using zeoTAl and then optimized using the General Utility Lattice Program.[41] A two-step strategy, first with conjugated gradients algorithm for OH^-, Na^+, Cs^+, and H_2O, keeping fixed the rest of the atoms, followed by the BFGS algorithm with full optimization, was employed. From the 20 optimizations, the lowest 5 energies of the zeolite systems were averaged, and the resulting energy was substituted in the corresponding equation (Table S2) to calculate the synthesis energy.

The synthesis energy (E_{syn}) for the inorganic cation-free system is defined as follows:[37]

$$E_{syn} = E[\text{zeo}(m,p) - p\text{SDA}] + 2{\cdot}(m + p)E_{H2O} - p{\cdot}E_{OSDA(OH)2} - m{\cdot}E_{(SiOH)4} - p{\cdot}E_{Si(OH)4} \quad (1)$$

where E[zeo(m,p) - pSDA] is the energy of the zeolite−OSDA pair, $E_{OSDA(OH)2}$ the energy of the 1,4-MPB^{2+} ion neutralized with two OH^- ions, and m and p the number of Si and Al atoms in the zeolite framework, respectively. The following synthesis equation was adjusted for each intermediate and final product (Table 2 and S2):

$$Na^+ + Cs^+ + SDA^{q+} + OH^- + H_2O + Si(OH)_4 + Al(OH)_3 \rightarrow [Na^+Cs^+(H_2O)(OH^-) - \text{zeo}(m,p)^{p-} - SDA^{q+}] \quad (2)$$

where q is 1 and 2 for inorganic and organic SDAs, respectively.

■ ASSOCIATED CONTENT

Supporting Information
The Supporting information is available free of charge at http://pubs.acs.org/doi/xx.xxxx/jacs.xxxxxxx.

Detailed computational procedures; the synthesis results and the calculated synthesis energies of the intermediates and final products; PXRD and mother liquor pH data; FE-SEM images and multinuclear MAS NMR spectra (PDF).

■ AUTHOR INFORMATION

Corresponding Author

Suk Bong Hong - Center for Ordered Nanoporous Materials Synthesis, Division of Environmental Science and Engineering, POSTECH, Pohang 37673, Korea; orcid.org/0000-0002-2855-1600; Email: sbhong@postech.ac.kr.

Authors

Jinjin Zeng - Center for Ordered Nanoporous Materials Synthesis, Division of Environmental Science and Engineering, POSTECH, Pohang 37673, Korea; orcid.org/0000-0003-3997-8658.
German Sastre - Instituto de Tecnologia Quimica (UPV-CSIC), Universidad Politecnica de Valencia, Valencia 46022, Spain; orcid.org/0000-0003-0496-6331.

Complete contact information is available at: https://pubs.acs.org/xx.xxxx/jacs.xxxxxxx

Author Contributions

All authors have given approval to the final version of the manuscript.

Notes

The authors declare no competing financial interest.

■ ACKNOWLEDGMENT

We acknowledge financial support from the National Research Foundation of Korea (2021R1A3A-3088711), GVA (PROMETEO/2021/077), MCIN (Severo Ochoa CEX-2021-001230-S), ASIC-UPV, and SGAI-CSIC for the use of computational facilities.

■ REFERENCES

(1) Vermeiren, W.; Gilson, J.-P. Impact of zeolites on the petroleum and petrochemcial industry. *Top. Catal.* **2009**, *52*, 1131-1161.

(2) Pérez-Botella, E.; Valencia, S.; Rey, F. Zeolites in adsorption processes: State of the art and future prospects. *Chem. Rev.* **2022**, *122*, 17647-17695.

(3) Barrer, R. M. *Hydrothermal Chemistry of Zeolites*; Academic Press: London, 1982.

(4) Thomson, R. W. Recent advances in the understanding of zeolite synthesis. In *Molecular Sieves Science and Technology*; Weitkemp, J., Karge, H. G., Eds.; Springer: Berlin, 1998; Vol. 1; 1-33.

(5) Corma, A.; Davis, M. E. Issues in the synthesis of crystalline molecular sieves: Towards the crystallization of low framework-density structures. *ChemPhysChem* **2004**, *5*, 304-313.

(6) Cundy, C. S.; Cox, P. A. The hydrothermal synthesis of zeolites: Precursors, intermediates and reaction mechanism. *Microporous Mesoporous Mater.* **2005**, *82*, 1-78.

(7) Park, M. B.; Lee, Y.; Zheng, A.; Xiao, F.-S.; Nicholas, C. P.; Lewis, G. J.; Hong, S. B. Formation pathway for LTA zeolite crystals synthesized via a charge density mismatch approach. *J. Am. Chem. Soc.* **2013**, *135*, 2248-2255.

(8) Grand, J.; Awala, H.; Mintova, S. Mechanism of zeolites crystal growth: new findings and open questions. *CrystEngComm* **2015**, *18*, 650-664.

(9) Mallette, A. J.; Shilpa, K.; Rimer, J. D. The current understanding of mechanistic pathways in zeolite crystallization. *Chem. Rev.* **2024**, *124*, 3416–3493.

(10) Dwyer, F. G.; Chu, P. ZSM-4 crystallization via faujasite metamorphosis. *J. Catal.* **1979**, *56*, 263-271.

(11) van Santen, R. A. The Ostwald step rule. *J. Phys. Chem.* **1984**, *88*, 5768-5769.

(12) Lewis, D. W.; Freeman, C. M.; Catlow, C. R. A. Predicting the templating ability of organic additives for the synthesis of microporous materials. *J. Phys. Chem.* **1995**, *99*, 11194-11202.

(13) Navrotsky, A.; Trofymluk, O.; Levchenko, A. A.; Thermochemistry of microporous and mesoporous materials. *Chem. Rev.* **2009**, *109*, 3885-3902.

(14) Hong, S. B.; Lear, E. G.; Wright, P. A. Zhou, W.; Cox, P. A.; Shin, C.-H.; Park, J.-H.; Nam, I.-S. Synthesis, structure solution, characterization, and catalytic properties of TNU-10: A high-silica zeolite with the STI topology. *J. Am. Chem. Soc.* **2004**, *126*, 5817-5885.

(15) Gramm, F.; Baerlocher, C.; McCusker, L. B.; Warrender, S. J.; Wright, P. A.; Han, B.; Hong, S. B.; Liu, Z. Ohsuna, T.; Terasaki, O. Complex zeolite structure solved by powder diffraction and electron microscopy. *Nature* **2006**, *444*, 79-81.

(16) Hong, S. B.; Min, H.-K.; Shin, C.-H.; Cox, P. A.; Warrender, S. J.; Wright, P. A. Synthesis, crystal structure, characterization, and catalytic properties of TNU-9. *J. Am. Chem. Soc.* **2007**, *129*, 10870-10885.

(17) Leonowicz, M. E.; Lawton, J. A.; Lawton, S. L.; Rubin, M. K. MCM-22: A molecular sieve with two independent multidimensional channel systems. *Science* **1994**, *264*, 1910-1913.

(18) Kubů, M.; Roth, W. J.; Greer, H. F.; Zhou, W.; Morris, R. E.; Přech, J.; Čejka, J. A new family of two-dimensional zeolites prepared from the intermediate layered precursor IPC-3P obtained during the synthesis of TUN zeolite. *Chem. Eur. J.* **2013**, *19*, 13937-13945.

(19) Guo, P.; Shin, J.; Greenway, A.; Min, J. G.; Su, J.; Choi, H. J.; Liu, L.; Cox, P. A.; Hong, S. B.; Wright, P. A.; Zou, X. A zeolite family with expanding structural complexity and embedded isoreticular structures. *Nature* **2015**, *524*, 74-78.

(20) Bae, J.; Cho, J.; Lee, J. H.; Seo, S. M.; Hong, S. B. EU-12: A small-pore, high-silica zeolite containing sinusoidal eight-ring channels. *Angew. Chem. Int. Ed.* **2016**, *55*, 7369-7373.

(21) Lee, H.; Shin, J.; Choi, W.; Choi, H. J.; Yang, T.; Zou, X.; Hong, S. B. PST-29: A missing member of the RHO family of embedded isoreticular zeolites, *Chem. Mater*. **2018**, *30*, 6619-6623.

(22) Lee, H.; Choi, W.; Choi, H. J.; Hong, S. B. PST-33: A four-layer ABC-6 zeolite with the stacking sequence AABC. *ACS Materials Lett.* **2020**, *2*, 981-985.

(23) Lee, H.; Shin, J.; Lee, K.; Choi, H. J.; Mayoral, A.; Kang, N. Y.; Hong, S. B. Synthesis of thermally stable SBT and SBS/SBT intergrowth zeolites. *Science* **2021**, *373*, 104-107.

(24) Zeng, J.; Lee, H.; Jo, D.; Mayoral, A.; Hong, S. B. Coupling different periodic building units for intergrowth zeolites. *J. Am. Chem. Soc.* **2024**, *146*, 13651-13657.

(25) Shin, J.; Jo, D.; Hong, S. B. Rediscovery of the importance of inorganic synthesis parameters in the search for new zeolites. *Acc. Chem. Res.* **2019**, *52*, 1419-1427.

(26) Flanigen, E. M. A review and new perspectives in zeolite crystallization. *Adv. Chem*. **1973**, *121*, 119−139.

(27) Gabelica, Z.; Blom, N.; Derouane, E. G. Synthesis and characterization of ZSM-5 type zeolites: III. A critical evaluation of the role of alkali and ammonium cations. *Appl. Catal.* **1983**, *5*, 221−248.

(28) Burton, A.; Accardi, R. J.; Lobo, R. F.; Falcioni, M.; Deem, M. W. MCM-47: A highly crystalline silicate composed of hydrogen-bonded ferrierite layers. *Chem. Mater*. **2000**, *12*, 2936-2942.

(29) Baerlocher, C.; McCusker, L. B. *Database of Zeolite Structures*; http://www.iza-structure.org/databases/ (accessed June 27, 2024).

(30) Ostwald, W. *Lehrbuch der Allgemeinen Chemie*; W. Engelmann, Leipzig, Germany, 1896; Vol. 2, Part 1.

(31) Zicovich-Wilson, C. M.; Gándara, F.; Monge, A.; Camblor, M. A. In situ transformation of TON silica zeolite into the less dense ITW: Structure-direction overcoming framework instability in the synthesis of SiO_2 zeolites. *J. Am. Chem. Soc.* **2010**, *132*, 3461-3471.

(32) Baerlocher, C.; Gramm, F.; Massüger, L.; McCusker, L. B.; He, Z.; Hovmöller, S.; Zou, X. Structure of the polycrystalline zeolite catalyst IM-5 solved by enhanced charge flipping. *Science* **2007**, *315*, 1113-1116.

(33) Casci, J. L.; Maberly, S.; Benazzi, E.; Rouleau, L.; Henney, R. P. NU-88 zeolite, a process for its preparation and catalytic application thereof. U.S. Patent 6,027,707, February 22, 2000.

(34) Lee, S.-H.; Lee, D.-K.; Shin, C.-H.; Park, Y.-K.; Wright, P. A.; Lee, W. M.; Hong, S. B. Synthesis, characterization, and catalytic properties of zeolites IM-5 and NU-88. *J. Catal.* **2003**, *215*, 151-170.

(35) Araya A.; Lowe, B. M. Zeolite EU-7. U.S. Patent 4,581,212, April 8, 1986.

(36) De Prins, M.; Verheyen, E.; Kerkhofs, S.; Hoffmann, A.; Vanbutsele, G.; Sree, S. P.; Radhakrishnan, S.; Van Tendeloo, L.; Breynaert, E.; Kirschhock, C. E. A.; Schütze, F.-W.; Martens, J. A. EU-7 zeolite: A synthetic BIK type zeolite with high hydrothermal stability. *Chem. Commun.* **2018**, *54*, 5626-5629.

(37) Altundal, O. F.; Leon, S.; Sastre, G. Different zeolite phases obtained with the same organic structure directing agent in the presence and absence of aluminum: The directing role of aluminum in the synthesis of zeolites. *J. Phys. Chem. C* **2023**, *127*, 10797−10805.

(38) Altundal, O. F.; Sastre, G. The directing role of aluminum in the synthesis of PST-21 (PWO), PST-22 (PWW), and ERS-7 (ESV) zeolites. *J. Phys. Chem. C* **2023**, *127*, 15648−15656.

(39) Bushuev, Y. G.; Sastre, G. Atomistic simulations of structural defects and water occluded in SSZ-74 zeolite. *J. Phys. Chem. C* **2009**, *113*, 10877−10886.

(40) Misturini, A.; Rey, F.; Sastre, G.: Molecular simulation of biobutanol recovery using LTA and CHA zeolite nanosheets with an external surface. *J. Phys. Chem. C* **2022**, *126*, 17680−17691.

(41) Gale, J. D. GULP: A computer program for the symmetry-adapted simulation of solids. *J. Chem. Soc.*, *Faraday Trans.* **1997**, *93*, 629-637.

Table of Contents (TOC)